2021

Design Optimization of 3mm and 5mm Copper Tube and Flat Fin Air-to-Water Heat Exchangers with Experimental Validation

Daniel Bacellar
Optimized Thermal Systems, Inc., dfbace@umd.edu

Dennis Nasuta
Optimized Thermal Systems, Inc.

Song Li
Optimized Thermal Systems, Inc.

Cara Martin
Optimized Thermal Systems, Inc.

Dale Powell
Copper Development

Design Optimization of 3mm and 5mm Copper Tube and Flat Fin Air-to-Water Heat Exchangers with Experimental Validation

Daniel BACELLAR[1], Dennis NASUTA[1*], Song LI[1], Cara MARTIN[1], Dale POWELL[2]

[1]Optimized Thermal Systems, Inc. Beltsville, MD
(nasuta@optimizedthermalsystem.com)

[2]Copper Development Association, Inc.
(dale.powell@copperalliance.us)

* Corresponding Author

ABSTRACT

The literature has extensively demonstrated the benefits of tube diameter reduction for enhancing airside thermal performance, increasing overall compactness and potential refrigerant charge reduction in air-to-refrigerant heat exchangers. The first part of this work consisted of a numerical design optimization of an air-to-water heat exchanger using 3mm and 5mm diameter tubes with same face and surface areas. The purpose is to demonstrate that when all geometric characteristics are kept constant, the smaller tube diameter has always greater thermal-hydraulic performance. The results showed that for the same air pressure drop, the 3mm diameter tube heat exchanger has up to 15% more capacity, while for same capacity the 5mm diameter tube heat exchanger has more than 60% greater pressure drop. The two selected designs, in addition to a reference 3mm design with greater fin density, were prototyped and tested in a temperature and humidity-controlled wind-tunnel. The prototypes were not an exact representation of the designs since the 3mm had reduced fin density, while the 5mm had increased fin density. These changes gave advantage to the 5mm in terms of capacity however, the experimental results clearly illustrated the superior overall thermal-hydraulic performance of the 3mm design which, even with reduced surface area, resulted in 5-10% better thermal-hydraulic ratio. The numerical prediction deviated from test data on average by 2.8% on heat load, and 14% on airside pressure drop.

Keywords: tube-fin heat exchanger, small diameter, optimization, experimental, validation

1. INTRODUCTION

The use of small diameter tube in tube-fin heat exchangers (HXs) has several benefits including better thermal performance, more compact surfaces, less material usage and lower refrigerant charge. The HVAC industry has followed such trend by moving from 9.52mm tubes to 7mm and 5mm, which are now common in many heat pumps and air conditioners. Manufacturing challenges and costs are currently the main factors holding back the use of tubes smaller than 5mm, however R&D continues, and progress has been made.

In the past decade, researchers developed general CFD-based correlations for airside characterization on small diameter (5mm or less) tubes with a variety of fin types: flat (Bacellar et al., 2014), wavy smooth and Herringbone (Bacellar et al., 2016), slit (Sarpotdar et al., 2016a) and louver (Sarpotdar et al., 2016b). While these tools provide great flexibility in exploring novel designs, little empirical data exists to this date. Nasuta et al. (2018) presented experimental data comparing against the louver and slits correlation predictions for 5mm tube samples. They investigated 8 distinct designs for each fin type and found that the correlation overpredicted pressure drop by 1.6% and 18% for louver and slit fins, respectively, while heat transfer coefficient was overpredicted by approximately 14% for both fin types. For the latter, the authors attributed the differences due to typical numerical deviations but also due to existing tube-fin contact resistance not captured by CFD-based correlations, and other experimental uncertainties enhanced under certain test conditions. Predicting contact resistance is difficult since it is subject to many factors such as tube diameter / thickness, fin collar size, material, type of joint (i.e. mechanically expanded, pressure expanded, or brazed), tolerances, and others. An experimental-analytical study applied to various fin types and mechanically expanded tubes showed that for 9.52mm tubes, the contact resistance accounts for 6-19% of the total airside thermal

resistance (Jeong et al., 2004). This same research group later published an identical study on 7mm tubes and found that the contact resistance accounted for 15-36% of the total airside thermal resistance (Jeong et al., 2006).

In the present study, a numerical investigation on both 5mm and 3mm tube and flat fin HXs is presented. The objective is to evaluate the thermal-hydraulic characteristics of different tube diameters when the HXs are geometrically equivalent, i.e. same face area, same airside heat transfer surface and equivalent in-tube mass flux. One 5mm and two 3mm tube prototypes were tested for validation purposes. All prototypes were manufactured with same process; tubes were pressure expanded.

2. MATERIALS & METHODS

2.1 Analysis Approach

This work used a 3mm tube, proof-of-concept, HX (referred as RD3S1T1) as a reference. A baseline performance for this HX - using hot water as working fluid - was estimated using a general purpose HX design tool (Jiang et al., 2006) and the flat fin correlations for small diameter tubes (Bacellar et al., 2014). The RD3S1T1 has a fin density of 28FPI, which is greater than that of the correlation range (10 to 24FPI), so a design optimization study was carried out to investigate optimum designs within the valid fin density range, under the same operating conditions. A similar study was conducted for 5mm tubes, however, constraining the airside surface area to be the same as the 3mm designs. Two designs from each study were selected for prototyping referred to as OD3S1T1 and OD5S1T1 for the 3mm and 5mm tube optimum designs, respectively. All three prototypes were then subject to testing in a closed-loop, temperature-controlled wind tunnel, under multiple operating conditions. In order to reduce uncertainties on the waterside data reduction, all HX's have smooth tubes.

2.1.1 Design Optimization

The baseline conditions were established as such that the heat capacitance rate ratio (C*) is approximately 0.2, the waterside is sufficiently in fully developed turbulent flow regime (Re~25,000) and the inlet approach temperature large enough (ΔT = 55°C) to result in significant deltas on both working fluids. The optimization studies used the exact same conditions, aiming to maximize heat load and minimize airside pressure drop (Table 1). Constraints were imposed only on geometry (face and surface areas), i.e. the optimum designs did not need to outperform the established reference. The design space was limited to transverse tube pitch, fin density and number of tube rows per bank, while the tube diameter, longitudinal-to-transverse pitch ratio, tube banks and number of counterflow circuits were fixed parameters (Table 1).

Table 1: Optimization Problem.

Objectives	Constraints	Variables	Fixed Parameters
$\max \dot{Q}$	$A_{face} = A_{face,reference}$	$1.5 \le P_t / D_o \le 3.0$	$D_o = [3,5] mm$
$\min \Delta P_{air}$	$0.98 \le A_o / A_{o,reference} \le 1.02$	$10 \le FPI \le 24$	$P_l / P_t = 0.433 (equilateral)$
		$10 \le N_r \le 40$	$N_b = 2$
			$N_c = 8 (D_o = 3); N_c = 3 (D_o = 5)$

2.1.2 Experimental Setup

The tests were conducted in a temperature and humidity-controlled wind tunnel (Figure 1) while using hot water as in-tube working fluid. Dry-bulb temperatures were measured through a 9-point and 25-point thermocouple (TC) grid at inlet and outlet of the coil, respectively. Additional instrumentation included two relative humidity sensors placed near to their respective TC grids. Static pressure difference across the coil and across a calibrated nozzle matrix were measured for pressure drop and airflow rate assessment.

In order to fully characterize the thermal-hydraulic performance of each HX, a 9-point test matrix with a combination of three water flow rates and three air flowrates was tested (Table 2). The flow rates were selected as such to cover a range of interest of air velocities and to ensure fully developed turbulent flow on the water side, while satisfying pump capacity and aiming to maintain high capacitance rate ratio (C*) to avoid temperature pinching.

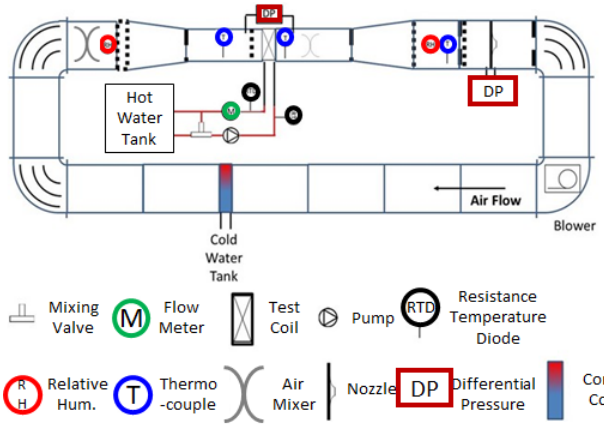

Parameter	Type	Range	Systematic Uncertainty
Water flow rate	Coriolis flow meter	0 to 700 g/s	0.5% of reading
Water inlet & outlet temperature	RTD	-100 to 400°C	±0.03 K
Air inlet temperature	9-point thermocouple	-200 to 200°C	±0.17 K
Air outlet temperature	25-point thermocouple	-200 to 200°C	±0.1 K
Coil air-side pressure drop	Differential pressure	1" WC	0.25% FS
Relative humidity (RH)	RH sensor	0-95%	±2%
Nozzle air-side pressure drop	Differential pressure	5" WC	0.25% FS

Figure 1: Setup Diagram.

Table 2: Test Matrix.

Test #	T_{water} °C	Water Flow Rate g/s	Re_{water} -	T_{air} °C	Air Flow Rate CFM (m/s)	C* -
#1	50	75	9000-14500	15	315 (2.3)	0.58
#2		100	12000-19700			0.43
#3		125	15000-25000			0.35
#4		75	9000-14500		450 (3.3)	0.83
#5		100	12000-19700			0.62
#6		125	15000-25000			0.50
#7		75	9000-14500		625 (4.6)	0.88
#8		100	12000-19700			0.86
#9		125	15000-25000			0.68

2.1.3 Test Data Reduction

Since there is only sensible heat load on the airside, a direct UA-LMTD method was employed to determine the global thermal resistance, which is broken down into both air and water convective thermal resistances and tube wall resistance (eq. (1)). The waterside resistance was estimated using the Gnielinski (1975) correlation (eq. (2)) for smooth tubes, while the airside effective heat transfer coefficient was directly extracted by the difference (eq. (3)). The actual heat transfer coefficient and fin effectiveness were retrieved by iterative calculations using the Schmidt (1949) method.

$$R_T = \left(\Delta T_{lm,test} / \dot{Q}_{test}\right) = R_{air} + R_{tube\_wall} + R_{water} \tag{1}$$

$$R_{water} = \left[\frac{k \cdot A_{water}}{D_i} \cdot \frac{\left((0.79\ln(\mathrm{Re}) - 1.64)^{-2}/8\right)\cdot(\mathrm{Re}-1000)\cdot \mathrm{Pr}}{1+12.7\left((0.79\ln(\mathrm{Re}) - 1.64)^{-2}/8\right)^{0.5}\left(\mathrm{Pr}^{2/3}-1\right)}\right]^{-1} \tag{2}$$

$$\eta_o \cdot h_{air} = A_o^{-1} \cdot \left(R_{total} - R_{water} - R_{tube\_wall}\right)^{-1} \tag{3}$$

3. RESULTS

3.1 Optimization Results

The optimization for the 3mm tube was unconstrained by surface area, however the selected design has similar surface area than the reference design (Figure 2). It is important to note that the reference design falls in a non-dominated region of the Pareto front for 3mm, which suggests that it is a good design; if the fin density was allowed to be greater than 24, it is possible that the Pareto front would have bridged the gap. For 5mm, on the other hand, solutions exhibited a Pareto front in clusters, and this is due to the surface area constraint imposed. Each cluster has similar fin densities and different tube patterns. All 5mm designs are dominated by the 3mm ones. With respect to the selected 3mm design, the 5mm with same pressure drop has 15% less capacity, while for the same capacity, the 5mm designs will have more than 60% greater pressure drop. The design with equivalent pressure drop was selected for prototyping. Like many studies before this, the advantages of small tubes in performance have been demonstrated but also in compactness and weight as shown in Figure 2 comparing the 3mm against the 5mm design.

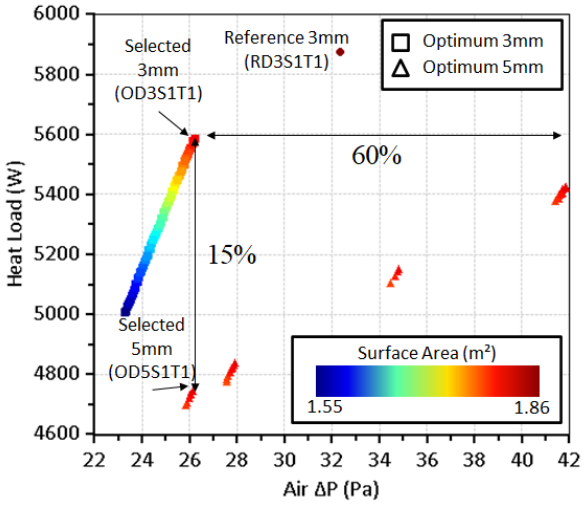

Coil	*Unit*	*OD5S1T1*	*OD3S1T1*	*RD3S1T1*
Tube				
D_o	m	0.005	0.003	0.003
L_t	m	0.277	0.224	0.252
W	m	0.022	0.016	0.014
N_r	-	18	32	32
Fins				
FPI	1/in	17.2	23.9	28
General Geometry				
A_{face}	m²	0.065	0.065 **(0%)**	0.065**(0%)**
A_o	m²	1.837	1.823 **(↓1%)**	1.858 **(↑1%)**
A_{cs}	m²	4.36E-05	4.25E-05 **(↓2.5%)**	4.25E-05 **(↓2.5%)**
M_{HX}	kg	0.728	0.500 **(↓32%)**	0.532 **(↓27%)**
A_o/V_{HX}	m²/m³	1272	1813 **(↑42%)**	2073 **(↑63%)**
Performance				
Q	W	4731.8	5562.5 **(↑18%)**	5876.8 **(↑24%)**
Q/V_{HX}	MW/m³	3.28	5.53 **(↑69%)**	6.55 **(↑100%)**
Air ΔP	Pa	26.1	26.1 **(0%)**	32.3 **(↑24%)**
h_{air}	W/m².K	75.6	98.7 **(↑31%)**	105.2 **(↑39%)**

Figure 2: Optimization Results.

3.2 Prototypes

While the actual prototypes (Figure 3) have the correct overall dimensions, they have different fin densities: the OD5S1T1 has 18.7FPI which corresponds to 7.3% surface area increase, while the OD3S1T1 has 20.8 FPI which corresponds to a 14.9% surface area decrease (Table 3). To account for these differences, new simulations were carried out for validation purposes.

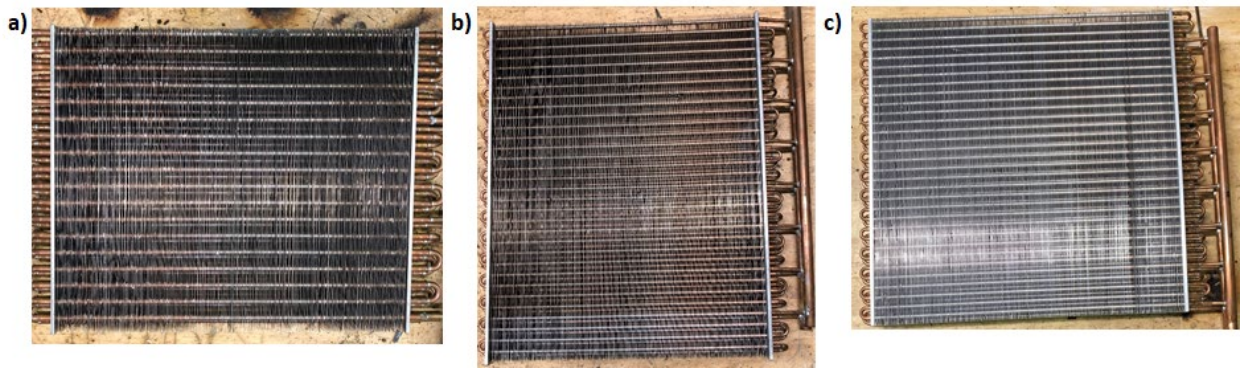

Figure 3: Prototypes: a) OD5S1T1; b) OD3S1T1; c) RD3S1T1.

Table 3: Prototypes Actual Geometry.

Coil		OD5S1T1 - Design **(Actual)**	OD3S1T1 - Design **(Actual)**	RD3S1T1 - Design **(Actual)**
D_o	m	0.005 **(0.005)**	0.003 **(0.003)**	0.003 **(0.003)**
FPI	in^{-1}	17.2 **(18.7) ↑8.2%**	23.9 **(20.8) ↓14.9%**	28 **(28.3) ↑0.3%**
A_o	m²	1.837 **(1.971) ↑7.3%**	1.823 **(1.575) ↓13.6%**	1.858 **(1.865) ↑0.3%**

3.3 Test Results

Table 4 to Table 6 summarize the test results for all three prototypes. The HX tests exhibited very good energy balances; no greater than 2.3% due to the strategic choice of the test matrix points that yield low impact from measurement uncertainties. As expected, the OD3S1T1 exhibited lower capacity than the other two due to reduced surface area, but the OD5S1T1, even with the largest surface area, was unable to match capacity with the RD3S1T1. From a thermal-hydraulic ratio – comparing overall and airside thermal conductance to airside pressure drop – the OD3S1T1 is still superior to the other designs even with reduced fin density (Figure 4), which is a good indication that the optimization found a design with tube configurations with greater performance.

Table 4: Summary Test Results for OD5S1T1.

Metric	Unit	#1	#2	#3	#4	#5	#6	#7	#8	#9
Energy Balance	%	-0.52%	0.87%	0.22%	1.37%	1.18%	1.12%	1.95%	1.94%	1.84%
Q	W	2863	3010	3119	3374	3604	3743	3876	4180	4366
ΔT_{water}	K	9.1	7.2	6.0	10.8	8.6	7.2	12.4	10.0	8.4
ΔT_{ml}	K	22.8	23.1	23.5	23.2	23.9	24.3	23.4	24.2	24.7
UA	W/K	125.3	130.2	133.0	145.2	150.7	154.0	165.6	172.9	177.0
h_{air}	W/m².K	72.5	74.3	75.2	85.9	87.7	88.7	100.4	102.9	104.0
$R_{air,total}$ / R_T	%	92.5%	93.9%	94.8%	91.3%	92.9%	94%	90%	91.8%	93%
ΔP_{air}	Pa	32.6	32.7	32.7	60.4	60.5	60.6	103.7	104.0	104.0

Table 5: Summary Test Results for OD3S1T1.

Metric	Unit	#1	#2	#3	#4	#5	#6	#7	#8	#9
Energy Balance	%	0.45%	0.39%	-0.76%	1.33%	0.51%	0.59%	1.35%	1.37%	1.31%
Q	W	2944	3142	3226	3471	3722	3882	3937	4302	4523
ΔT_{water}	K	9.4	7.5	6.2	11.1	8.9	7.4	12.6	10.3	8.7
ΔT_{ml}	K	22.5	22.9	23.1	23.0	23.6	23.9	23.2	24.0	24.4
UA	W/K	131.1	137.1	139.9	150.6	157.8	162.3	170.0	179.5	185.4
h_{air}	W/m².K	91.1	93.7	94.6	106.3	109.2	110.9	121.9	125.8	128.1
$R_{air,total}$ / R_T	%	91.3	92.9	93.9	89.9	91.7	92.9	88.5	90.6	91.9
ΔP_{air}	Pa	28.4	28.4	28.5	52.1	52.2	52.3	89.4	89.6	89.7

Table 6: Summary Test Results for RD3S1T1.

Metric	Unit	#1	#2	#3	#4	#5	#6	#7	#8	#9
Energy Balance	%	-2.33%	-1.81%	-2.12%	-0.80%	-1.16%	-0.65%	-0.70%	-0.67%	-0.62%
Q	W	3360	3581	3780	3934	4308	4509	4498	4964	5286
ΔT_{water}	K	10.7	8.6	7.2	12.6	10.3	8.6	14.4	11.9	10.1
ΔT_{ml}	K	21.0	20.9	21.3	21.4	21.9	22.1	21.7	22.3	22.8
UA	W/K	160.2	171.4	177.3	184.0	196.3	204.2	207.0	222.3	232.0
h_{air}	W/m².K	97.8	103.0	105.4	114.9	120.2	123.5	132.0	138.8	142.8
$R_{air,total}$ / R_T	%	90.5%	92%	93.1%	88.9%	90.8%	92%	87.5%	89.5%	90.9%
ΔP_{air}	Pa	46.7	47.1	47.1	84.0	84.2	84.2	141.7	142.2	142.4

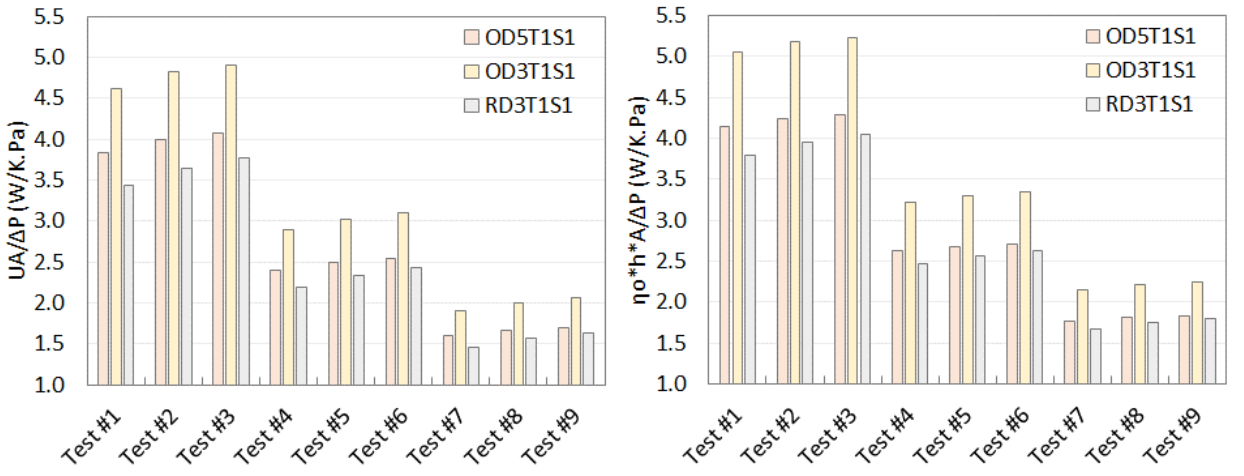

Figure 4: Experimental Thermal-Hydraulic Performance.

3.4 Validation

New simulations were carried out to reflect the exact test conditions and modified fin densities. Very good agreement was found on all three prototypes in all test conditions. The predicted air and water outlet temperatures were within 1°C. The heat load was predicted within 8% for all test points; the OD3S1T1 exhibited the largest deviations and for every point they were underpredicted (Figure 6). The same was not observed for pressure drop, where the correlations predicted reasonably well for both OD3S1T1 and OD5S1T1, but it consistently underpredicted by 20-25% for RD3S1T1. The reason for the later maybe due to the fact the fin density is outside the correlation range. Pressure drop is typically well predicted for low air velocities and diverges for higher velocities as illustrated in Figure 7.

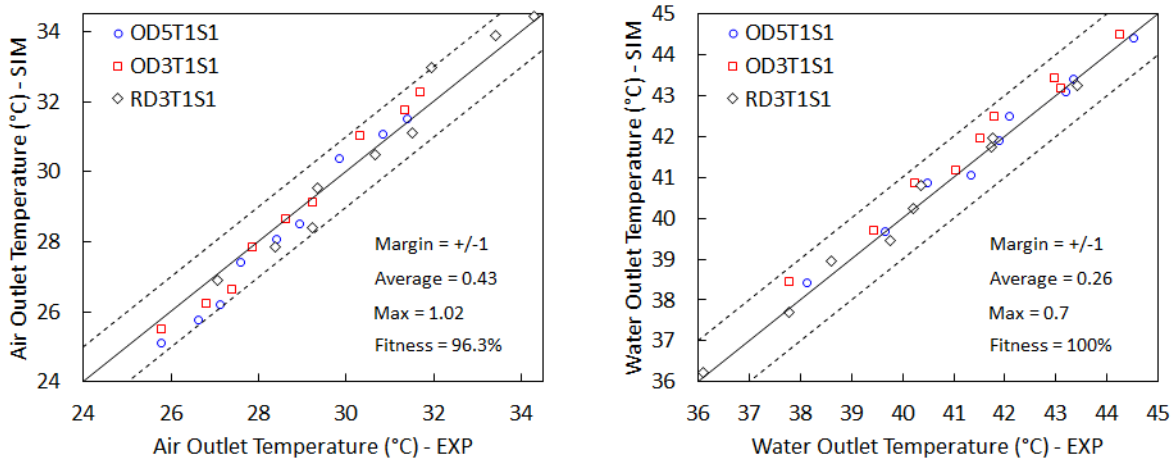

Figure 5: Experimental Validation: Air and Water Outlet Temperatures.

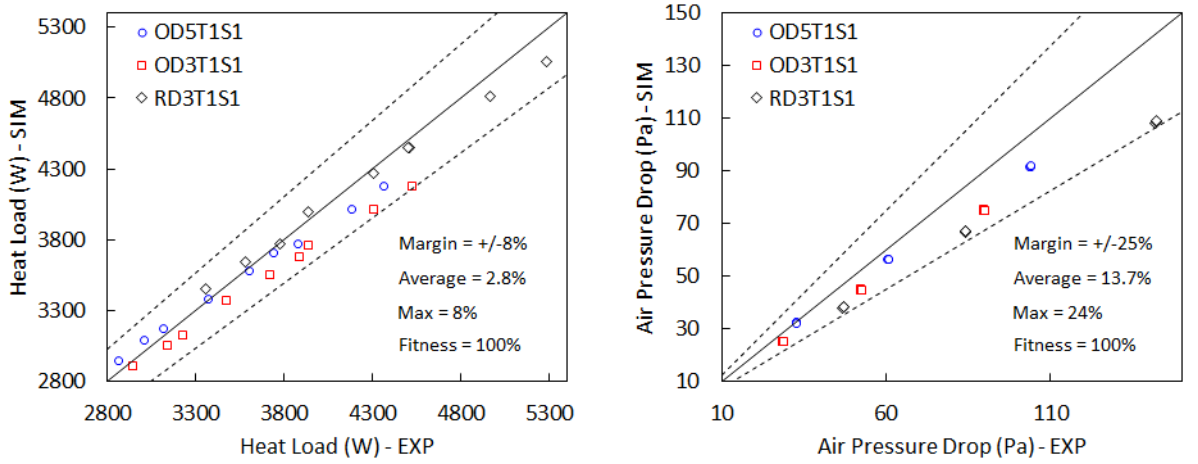

Figure 6: Experimental Validation: Heat Load and Airside Pressure Drop.

Finally, the airside heat transfer coefficient exhibited a somewhat good agreement, but the simulation and experimental trends are seemingly counter-intuitive. CFD and CFD-based correlations tend to over predict airside heat transfer coefficient, since they do not take into account other parasitic resistances such as tube-fin contact. The curves cross at a certain velocity (Figure 8) which means they do not consistently overpredict or underpredict. Another interesting difference, which was observed on all three designs, is the curvature slope, or power rate at which the heat transfer varies with the air velocity where the experimental curves grow at grater rate. For lower velocities, the correlations tend to underpredict, but at higher velocities the thermal performance is actually greater than expected.

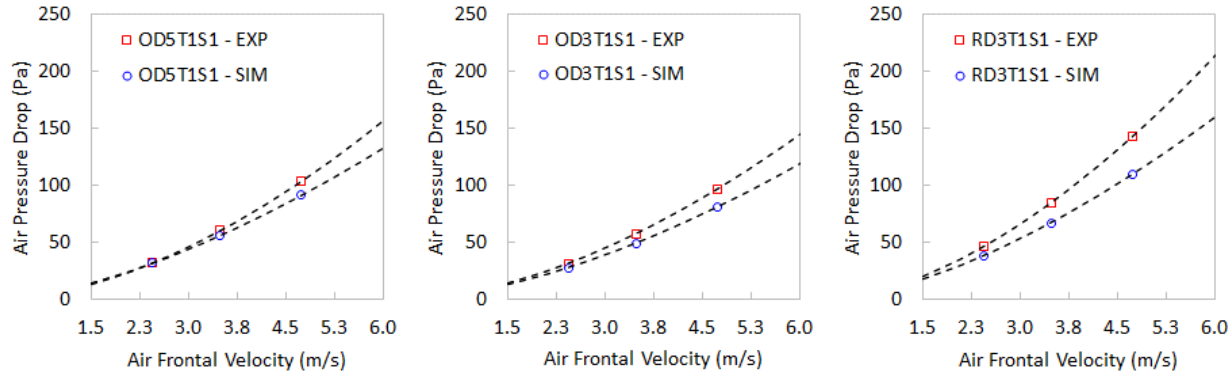

Figure 7: Airside Pressure Drop.

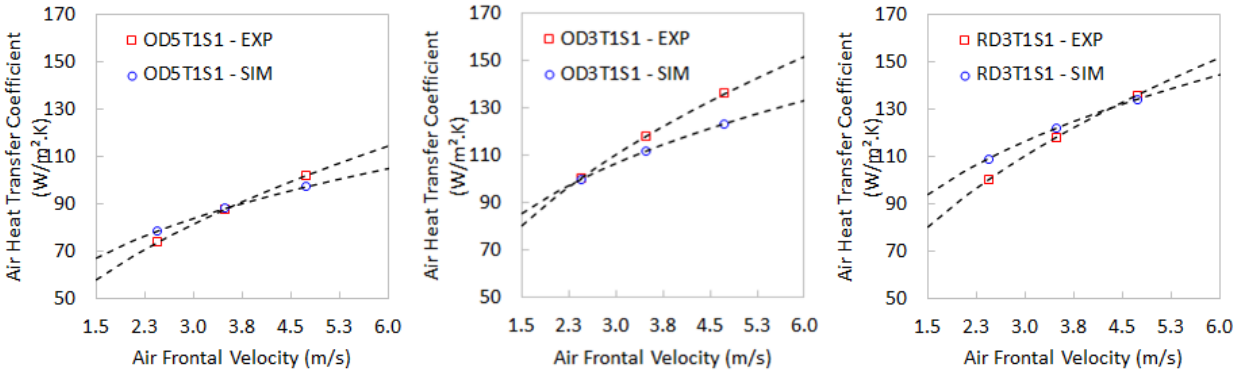

Figure 8: Airside Heat Transfer Coefficient.

4. CONCLUSIONS

This work is part of a comprehensive R&D effort in the investigation of using tube diameters smaller than 5mm for HVAC applications. In this paper a numerical optimization was presented illustrating how, under equivalent geometry characteristics, a 3mm tube has greater advantage on thermal-hydraulic performance. The results showed that for same air pressure drop, the 3mm has up to 15% more capacity, while for same capacity the 5mm has more than 60% greater pressure drop. The prototypes were not an exact representation of the designs since the 3mm had reduced fin density, while the 5mm had increased fin density. These changes gave advantage to the 5mm in terms of capacity however, the experimental results clearly illustrated the superior overall thermal-hydraulic performance of the 3mm design which, even with reduced surface area, resulted in 5-10% better thermal-hydraulic ratio. Furthermore, the test results served as the first available data for validation of the flat fin and tube correlation. The numerical prediction deviated from test data on average by 2.8% on heat load, and 14% on airside pressure drop. This work is the first known, to the best of the authors' knowledge, to perform experimental tests on a 3mm tube HX. The future work will include performing tests on these prototypes under wet and frost conditions to evaluate the differences in performance degradation between 3mm and 5mm tubes. Additional tests with superhydrophobic coating will also be carried out, to evaluate the impact on moisture retention and ice shedding.

NOMENCLATURE

A_o	Airside Surface Area	(m^2)
A_{cs}	Water Flow Total Cross-Section Area	(m^2)
A_{face}	Face Area	(m^2)
A_{water}	Waterside Surface Area	(m^2)
C*	Heat Capacitance Ratio	(-)
D_i	Tube Inner Diameter	(m)
D_o	Tube Outer Diameter	(m)
EXP	Experimental	(-)
FPI	Fins Per Inch	(in^{-1})
h	Convective Heat Transfer Coefficient	($W/m^2.K$)
k	Thermal Conductivity	(W/m.K)
L_t	Tube Length	(m)
M_{HX}	Heat Exchanger Mass	(kg)
N_b	Tube Banks	(-)
N_c	Number of Circuits	(-)
N_r	Tube Rows per Bank	(-)
P	Pressure	(Pa)
P_l	Tube Longitudinal Pitch	(m)

P_t	Tube Transverse Pitch	(m)
Q	Heat Load	(W)
R	Thermal Resistance	(K/kW)
Re	Reynolds Number	(-)
SIM	Simulation	(-)
T	Temperature	(K)
u	Air Velocity	(m/s)
UA	Global Thermal Conductance	(W/K)
V_{HX}	Heat Exchanger Footprint Volume	(m^3)
W	Heat Exchanger Depth	(m)
ΔP	Pressure Drop	(Pa)
ΔT	Temperature Difference	(K)
ΔT_{ml}	Log-Min Temperature Difference	(K)
η_o	Fin Effectiveness	(-)

REFERENCES

Bacellar, D., Aute, V., & Radermacher, R. (2014). CFD-Based Correlation Development For Air Side Performance Of Finned And Finless Tube Heat Exchangers With Small Diameter Tubes. *15th International Refrigeration and Air Conditioning Conference at Purdue.* West Lafayette, IN.

Bacellar, D., Aute, V., & Radermacher, R. (2016). CFD-Based Correlation Development for Air Side Performance of Wavy Fin Tube Heat Exchangers using Small Diameter Tubes. *16th International Refrigeration and Air Conditioning Conference at Purdue.* West Lafayette, IN.

Jeong, J., Kim, C. N., & Youn, B. (2006). A study on the thermal contact conductance in fin–tube heat exchangers with 7 mm tube. *International Journal of Heat and Mass Transfer*, 1547–1555.

Jeong, J., Kim, C. N., Youn, B., & Kim, Y. S. (2004). A study on the correlation between the thermal contact conductance and effective factors in fin–tube heat exchangers with 9.52 mm tube. *International Journal of Heat and Fluid Flow*, 1006–1014.

Jiang, H., Aute, V., & Radermacher, R. (2006). CoilDesigner: a general-purpose simulation and design tool for air-to-refrigerant heat exchangers. *International Journal of Refrigeration, 29*(4), 601-610.

Nasuta, D., Li, S., Hwang, Y., & Martin, C. (2018). Experimental Validation of CFD-Based Correlations for 5 mm Louver- and Slit-Fin Heat Exchangers: Lessons Learned. *17th International Refrigeration and Air Conditioning Conference at Purdue.* West Lafayette, IN.

Sarpotdar, S., Nasuta, D., & Aute, V. (2016). CFD Based Comparison of Slit Fin and Louver Fin Performance for Small Diameter (3mm to 5 mm) Heat Exchangers. *16th International Refrigeration and Air Conditioning Conference at Purdue.* West Lafayette, IN.

Sarpotdar, S., Nasuta, D., & Aute, V. (2016). CFD-Based Airside Heat Transfer and Pressure Drop Correlation Development for Small Diameter (3 mm to 5 mm) Louver Fin Heat Exchangers. *16th International Refrigeration and Air Conditioning Conference at Purdue.* West Lafayette.

ACKNOWLEDGEMENT

This work was supported by the Copper Development Association, Inc. The authors would also like to acknowledge BurrOAK Tool® for providing the manufacturing means and building the small diameter tube prototypes.